Shear-induced mesostructures in biaxial liquid crystals

Sarthok Sircar* and Qi Wang†
Department of Mathematics, University of South Carolina, Columbia, South Carolina 29208, USA
(Received 13 April 2008; published 8 December 2008)

We study nematodynamics of a mesoscopic system consisting of sheared biaxial liquid crystalline polymers using a hydrodynamical kinetic theory. We solve the governing Smoluchowski equation using the Galerkin method in selected regions of the material parameter space and a range of accessible shear rates to investigate stable mesoscopic states and robust structures. The imposed shear flow breaks the rotational symmetry in the quiescent state to induce truly biaxial flow-aligning steady states, logrolling states, out-of-plane steady states, exotic time-periodic motions, and chaotic motions in different regimes of material parameters and shear rates.

DOI: 10.1103/PhysRevE.78.061702 PACS number(s): 61.30.Jf, 61.30.Cz, 61.30.Vx, 61.72.Lk

I. INTRODUCTION

Orientational dynamics of nematic liquid crystals in the presence of an external field is the fundamental mechanism for numerous modern technologies ranging from display devices and ultrafast switches to the processing of ultrahigh strength, high-performance materials [1]. Theories and experiments have been focused on uniaxial liquid crystals and have improved one's understanding of the soft matter significantly in the past 40 years [1–3]. Recently, attention has started shifting to the biaxial liquid crystal whose molecules exhibit reduced reflective symmetry (ellipsoidal or brick-shaped molecules) or reduced directional reflective symmetry (V-shaped, bent-core, or banana-shaped molecules [4]). Much of the experimental effort on biaxial liquid crystals is being made to understand the phases of the relatively new biaxial liquid crystals since their predicted existence and actual fabrication [5].

This class of liquid crystals is promising in that they can be used to increase the switching speed in already fast liquid crystal-based nanoswitches, to improve display quality in demanding applications, or to fabricate novel high-performance materials of enhanced properties. Flow-processing is a traditional means of fabricating high-performance materials made of liquid crystal polymers. Various fascinating phenomena have already been reported in different flow regimes during processing of uniaxial liquid crystal polymers, such as the flow-induced alignment, defect-infested domains, optical turbulence, defect formation and annihilation, defect interaction, domain walls, time-periodic motions, etc. [3,6]. In this paper, we report a set of mesoscopic states, either steady or time-dependent in sheared biaxial liquid crystal polymers, to supplement the already impressive list of shear-induced structures and transitions in flows of liquid crystals [6,7].

In a series of seminal papers, Virga *et al.* carefully studied the equilibrium phase diagram of a class of biaxial liquid crystals using mean-field theories based on a generalized Straley's interaction potential [8,9]. They identified universal features in biaxial liquid crystals encompassing various uniaxial and biaxial phases, phase transition sequences, tricritical points, and triple points in the material parameter space. Our aim in this paper is to explore how the imposed shear flow perturbs the existing biaxial phases via symmetry breaking to give rise to stable steady states (phases) as well as stable time-dependent motions and structures in selected regimes of material parameters and shear rates.

II. THEORY AND NUMERICS

The suitable framework to study mesosopic dynamics of the biaxial liquid crystal is the kinetic theory [2]. Let $f(\Omega,t)$ be the orientational probability density function (PDF) of the ellipsoidal (or brick-shaped), rigid biaxial nematogen, where $\Omega=(\alpha,\beta,\gamma)$ denotes the Euler angle triplet describing the instantaneous orientation of the molecular axes $(\mathbf{m},\mathbf{n},\mathbf{k})$ with respect to the fixed Cartesian frame (x,y,z). Here, we identify $\mathbf{m}$ as the longest semiaxis of length a, $\mathbf{n}$ the second longest of length b, and $\mathbf{k}$ the shortest of length c of the ellipsoidal molecule. The kinetic or the Smoluchowski equation is given by

$$\frac{\partial}{\partial t}f=-\mathbf{L}D_r\cdot\left(\mathbf{L}f+\frac{1}{k_BT}f\mathbf{L}\mathcal{U}\right)+\mathbf{L}\cdot(\mathbf{g}f), \tag{1}$$

where D_r is the nondimensional rotational diffusivity (assumed constant) [10,11]; $\mathbf{L}=\frac{\mathbf{x}}{i}\times\frac{\partial}{\partial\mathbf{x}}$ is the angular momentum operator; k_B is the Boltzmann constant; T is the absolute temperature; $\mathbf{g}$ is the torque due to the flow given by

$$\mathbf{g}=i\left(\frac{\mathbf{m}}{r_b^2+r_c^2}[\boldsymbol{\nabla}\mathbf{v}:(r_b^2\mathbf{nk}-r_c^2\mathbf{kn})]+\frac{\mathbf{n}}{1+r_c^2}[\boldsymbol{\nabla}\mathbf{v}:(r_c^2\mathbf{km}-\mathbf{mk})]\right.$$
$$\left.+\frac{\mathbf{k}}{1+r_b^2}[\boldsymbol{\nabla}\mathbf{v}:(\mathbf{mn}-r_b^2\mathbf{nm})]\right), \tag{2}$$

$r_b=\frac{b}{a}$, $r_c=\frac{c}{a}$ are the two aspect ratios of the ellipsoidal molecule, and $\boldsymbol{\nabla}\mathbf{v}$ is the velocity gradient of the velocity field $\mathbf{v}$. $\mathcal{U}$ is the excluded volume potential given by

$$\mathcal{U}=-\frac{3}{2}Nk_BT[\xi_0\mathbf{M}:\mathbf{mm}+\gamma_0(\mathbf{N}:\mathbf{mm}+\mathbf{M}:\mathbf{nn})+\lambda_0\mathbf{N}:\mathbf{nn}], \tag{3}$$

where $\mathbf{M}=\langle\mathbf{mm}\rangle$ and $\mathbf{N}=\langle\mathbf{nn}\rangle$ are the second moment tensors of $\mathbf{m}$ and $\mathbf{n}$ with respect to the PDF, respectively. The material parameters $(\xi_0,\gamma_0,\lambda_0)$ are linearly related to the parameters (γ,λ) of Straley's potential [12] as follows:

*sircars@math.sc.edu; URL: www.math.sc.edu/~sircars
†qwang@math.sc.edu

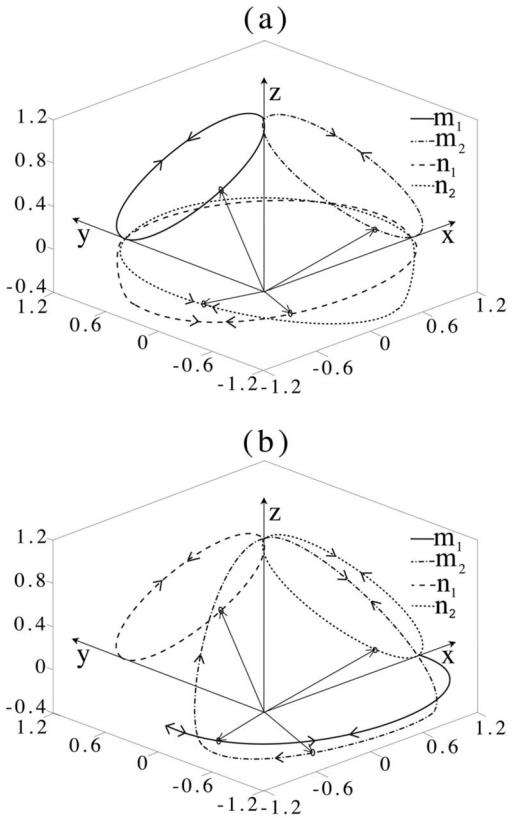

FIG. 1. Time-periodic motions. (a) Mixed-kayaking. Period: $T=4.98$. Parameter values Pe=7.6, $N=7.84$, $\gamma=0.081\,67$, and $\lambda=0.5$. (b) Fluttering-kayaking. Period: $T=4.92$. Parameter values Pe=9.7, $N=7.84$, $\gamma=0.081\,67$, and $\lambda=0.5$.

$$\xi_0 = 1 + 2\gamma + \lambda, \quad \gamma_0 = 2(\gamma + \lambda), \quad \lambda_0 = 4\lambda. \tag{4}$$

The dimensionless flow field for the simple shear in the Cartesian coordinate is given by

$$\mathbf{v} = \mathrm{Pe}(y,0,0), \tag{5}$$

where Pe is the Peclet number (the dimensionless shear rate). We employ a Wigner function based Galerkin-spectral method to solve the Smoluchowski equation numerically, in which the PDF is discretized by [6,7]

$$f(t,\Omega) = \sum_{L=0,|m|,|n|\leqslant L}^{L_0} C_{Lmn}(t)\mathcal{D}^L_{mn}(\Omega), \tag{6}$$

where $C_{Lmn}(t)$ are the time-dependent generalized Fourier coefficients and $\mathcal{D}^L_{mn}(\Omega)$ are the Wigner functions. We solve for the coefficients $C_{Lmn}(t)$ with the initial conditions $C_{Lmn}(0)$ obtained at $f(0,\Omega)=f_0(\Omega)$, where $f_0(\Omega)$ is the equilibrium PDF [8,13,14]. In the calculations, we use $L_0=10$ and the four-step Runge-Kutta scheme with the step size $\Delta t=10^{-3}$ to advance the system in time.

III. NUMERICAL RESULTS AND DISCUSSIONS

Due to the excluded volume interaction, a biaxial molecule in liquid crystal flows can feel an elastic torque, which vanishes in equilibrium. When shear is imposed, however, a shear-induced torque is exerted on the biaxial molecule to break the mesoscopic symmetry in equilibrium. The impact of the shear-induced torque on a single molecule is to rotate the ellipsoidal molecule in the flow. The shear-induced torque competes with the elastic restoring torque to decide the mesoscopic state of the ellipsoidal ensemble. Various new states and motions then arise out of the balance-imbalance between the competing elastic and shear-induced torque under shear.

Our numerical studies are carried out in the range of the shear strength $0.0 \leqslant \mathrm{Pe} \leqslant 14.0$ and for liquid crystalline polymer (LCP) concentrations $N=4.9$, 5.5, 6.28, and 7.84. Based on the equilibrium phase behavior in the system, we divide the admissible material parameters in the (γ,λ) space into four regions: region A: $\lambda \geqslant 1.0$, where the excluded volume interaction is highly biaxial [9]; region B: the region inside the space $\gamma^2 \leqslant \lambda < 1.0$ and bounded below by the tricritical curve (C_1C_3 in [9]), where a first order, temperature-induced, phase transition from the *isotropic*→*biaxial* phase was reported in [8,9]; the nature of this transition changes to a second order transition from the *isotropic*→*uniaxial*→*biaxial* phase, across the tricritical curve C_1C_3 in region C; region C: the region inside the space $\lambda \geqslant \gamma^2$ and bounded above by C_1C_3; and region D: $0 \leqslant \lambda < \gamma^2$; $|2\gamma| \leqslant 1+\lambda$, where the excluded volume potential is nonconvex. According to [9], the excluded volume potential in regions A–C are attractive and partly repulsive in region D. A detailed exercise in region D showed that the equilibrium free energy may not have a global minimum and hence the steady-state solution has to be obtained via a minimax principle [9,15].

Normally, the mesoscopic orientational information in kinetic theories is described by the second moments. For the autocorrelation matrix or the second moment **M**, we define its major director $\mathbf{m}_1$ as the unit eigenvector corresponding to its largest eigenvalue. We note that the eigenvalue of **M** measures the degree of orientation of the long molecular axis **m** with respect to the direction of the corresponding eigenvector. For the other autocorrelation matrices or second moments **N** and **K**, analogous definitions apply. For example, the major director of **N** is denoted by $\mathbf{n}_1$. In all our calculations, the degree of orientation of **m** with respect to $\mathbf{m}_1$ is always the largest and, therefore, $\mathbf{m}_1$ is the distinguished direction in the mesoscopic LCP system. When both $\mathbf{m}_1$ and $\mathbf{n}_1$ are on the (x,y) plane, the angle that $\mathbf{m}_1$ makes with the x axis is known as the Leslie angle and the one $\mathbf{n}_1$ makes with the y axis is called the secondary Leslie angle.

In region A, at low and intermediate Pe, the elastic torque balances the shear-induced torque to favor the logrolling (**LR**) steady state, where $\mathbf{m}_1$ aligns in the vorticity direction. As Pe increases beyond a critical value, the flow-aligning (**FA**) steady state prevails, where the major director $\mathbf{m}_1$ aligns in the proximity of the flow direction. In both steady states, the major director $\mathbf{n}_1$ stays on the (x,y) plane. Apparently, the elastic torque required to sustain a LR state is smaller than that required for a FA state. In both FA and LR states, the secondary Leslie angle forms a negative angle with the velocity gradient direction. In addition, the Leslie angle in the FA state is positive and the magnitudes of the two Leslie angles in the FA state tend to zero as $\mathrm{Pe}\to\infty$. The

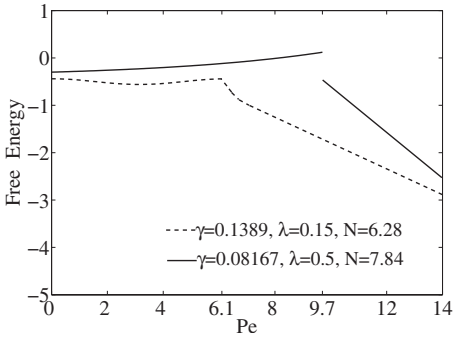

FIG. 2. Time-averaged free energy density versus Pe. The solid line is at $N=7.84$ and $(\gamma,\lambda) \in$ region B. A first order transition at Pe=9.7 is observed. The dashed line is at $N=6.28$ and $(\gamma,\lambda) \in$ region C. A second order transition at Pe=6.1 is shown.

transitional state from logrolling to flow-aligning is an out-of-plane steady state (OS) existing in a small transitional interval of Pe, where major directors $\mathbf{m}_1$ and $\mathbf{n}_1$ leave the flow velocity-gradient plane. The value of this critical Pe increases with the LCP concentration (N) because the excluded volume interaction becomes stronger at higher values of N. Hence the sequence of orientational response in this region as Pe increases is **LR**→**OS**→**FA**. This is reminiscent of the flow-driven state transition in uniaxial liquid crystals predicted using the Doi-Hess kinetic theory in some concentration regime [2,6,7].

Another important change that the imposed shear brings about is the symmetry breaking among the second moment tensors. It is widely believed that **M** and **N** commute in the quiescent state [9]. However, this is no longer true when shear is imposed. For instance, **M** and **N** share the vorticity axis as the common eigenvector direction in the **LR** and **FA** state, but the two tensors are noncommutative signifying a shear-induced symmetry breaking. It is even more pronounced in the transitional out-of-plane steady states, where all eigenvectors of **M** are skewed with those of **N** indicating additional symmetry breaking.

In region B, at high concentration ($N=5.5$, 6.28, and 7.84), $\mathbf{m}_1$ changes its alignment from the **LR** state at a low

TABLE I. Second column: Shear strength corresponding to period doubling bifurcations. Third column: Feigenbaum number (F) which approaches the limit $F \to 1.958$, a typical feature of harmonic cascading.

Label	Pe	$F=\frac{\mathrm{Pe}_i-\mathrm{Pe}_{i-1}}{\mathrm{Pe}_{i+1}-\mathrm{Pe}_i}$
PDL_1	1.161	
PDL_2	1.225	1.575
PDL_3	1.266	1.819
PDL_4	1.289	1.951
PDL_5	1.300	
PDR_1	2.472	
PDR_2	2.381	2.299
PDR_3	2.341	1.988
PDR_4	2.321	

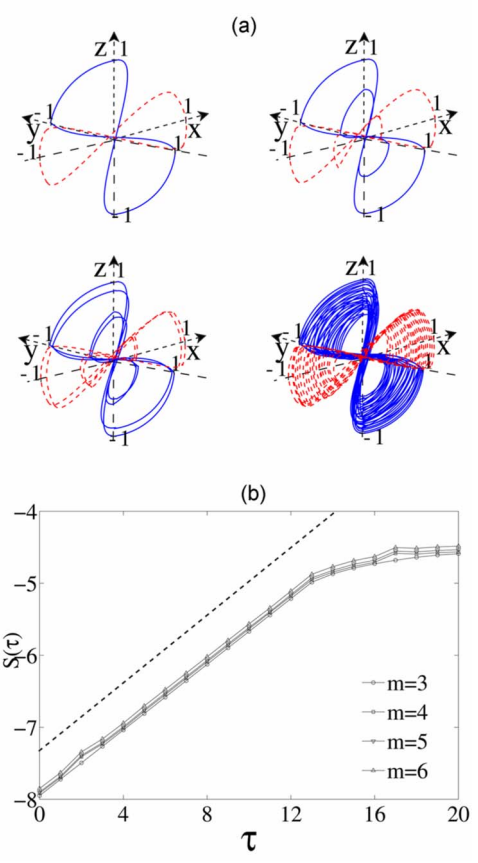

FIG. 3. (Color online) (a) The trajectory of the eigenvectors $\mathbf{m}_1$ (solid blue) and $\mathbf{n}_1$ (dashed red) after an initial transient. The parameter values are $N=4.9$, $\gamma=0.45$, $\lambda=0.009\,365\,4$, and (i) Pe=1.15; (ii) Pe=1.22; (iii) Pe=1.26; and (iv) Pe=1.32. (b) Stretching factor (details in [16]) versus the iteration time at different embedding dimensions "m" and Pe=2.00. The starting distance between any two trajectories is $\epsilon=0.002$. The dashed line indicates the slope at intermediate time.

Pe to the **FA** state at a high Pe via a couple of exotic out-of-plane time periodic motions termed as the mixed-kayaking (**MK**) and the fluttering-kayaking (**FK**) motion at intermediate Pe, depicted in Fig. 1. The **MK** motion is a tilted kayaking of $\mathbf{m}_1$ combined with the full kayaking of $\mathbf{n}_1$ [6,7]. In the **MK** phase, $\mathbf{m}_1$ and $\mathbf{m}_2$ (the second eigenvector

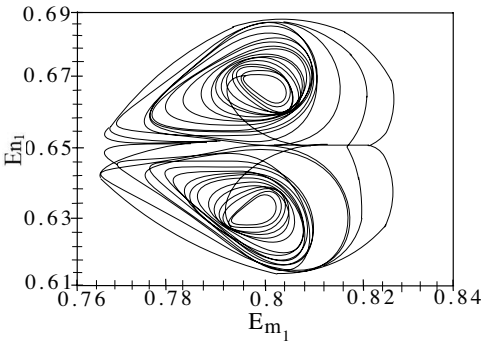

FIG. 4. Eigenvalues corresponding to the eigenvectors $\mathbf{m}_1$ and $\mathbf{n}_1$ after an initial transient in a chaotic motion. The parameter values are $N=4.9$, $\gamma=0.45$, $\lambda=0.009\,365\,4$, and Pe=1.32.

of **M**) collectively go through a coordinated tilted motion about their respective tilted axis; whereas $\mathbf{n}_1$ and $\mathbf{n}_2$ (the second eigenvector of **N**) rotate about the vorticity axis in a weakly nonplanar fashion, imitating a full-blown kayaking motion against the flow velocity-gradient plane. In the **FK** phase, $\mathbf{m}_1$ wags in the flow velocity-gradient plane while $\mathbf{m}_2$ goes through a truly nonplanar circular motion. The coordinated motion of $\mathbf{m}_1$ and $\mathbf{m}_2$ is reminiscent of the fluttering fall of a leaf or a feather in the air. In the meantime, $\mathbf{n}_1$ and $\mathbf{n}_2$ rotate around two tilted axes coordinately, analogous to the tilted kayaking. In the **MK** and the **FK** motion, the orbits of the pair of directors going through the tilted kayaking ($\mathbf{m}_1$ and $\mathbf{m}_2$ in MK and $\mathbf{n}_1$ and $\mathbf{n}_2$ in FK, respectively) osculate each other near the vorticity axis. The eigenframes of **M** and **N** are skewed in the time-periodic motion and the angle between $\mathbf{m}_1$ and $\mathbf{n}_1$ oscillates between 40° and 140° within a period. The degrees of orientation about the rotating directors fluctuate as well. In the absence of any out-of-plane steady state (**OS**) in this region, there is an abrupt transition of the **MK** state to the **FK** state which resembles a first order "phase transition" since the time-averaged free energy density exhibits an abrupt change from the **MK** state to the **FK** state shown in Fig. 2. The sequence of phase changes in this region as Pe increases follows **LR**$\rightarrow$**MK**$\rightarrow$**FK**$\rightarrow$**FA**.

In region C, the state at concentrations $N=5.5$, 6.28, and 7.84 changes gradually in the sequence **LR**$\rightarrow$**MK**$\rightarrow$**OS**$\rightarrow$**FK**$\rightarrow$**FA** as Pe increases. The existence of the out-of-plane steady state (**OS**) in the cascade implies that the transition of $\mathbf{m}_1$ from the out-of-plane unsteady **MK** phase to the partly in-plane unsteady **FK** phase is a continuous (or *second order*) phase-motion transition. This fact is corroborated by the continuous free-energy diagram in Fig. 2.

In region D, we observe two different sequences of states as Pe varies. At $\gamma=0.161\,98$, $\lambda=0.009\,365\,4$, and $N=5.5$, 6.28, and 7.84, we have the sequence **MK**$\rightarrow$**OS**$\rightarrow$**FK**$\rightarrow$**FA** and at $\gamma=0.45$, $\lambda=0.009\,365\,4$, and $N=4.9$ the sequence is **MK**$\rightarrow$**CH**$\rightarrow$**FK**$\rightarrow$**FA**, where **CH** stands for the chaotic state. The LR state at small Pe is absent in this region because the partly repulsive excluded volume interaction is weakly biaxial (smaller value of λ) such that the shear-induced torque dominates. As Pe increases, the elastic torque due to the mesoscopic structure enhances so that a balance is reached at high Pe leading to the steady FA state.

The chaotic solution (**CH**) arises at $N=4.9$ from the periodic **MK** state, inside the Peclet window $1.15 \leqslant \mathrm{Pe} \leqslant 2.5$. The solution shows period-doubling bifurcations, which leads to a harmonic cascade (see Table I), starting from a periodic rotation of $\mathbf{m}_1$ about a tilted axis. Figure 3(a) shows the evolution of $\mathbf{m}_1$ and $\mathbf{n}_1$ in this chaotic regime, where two attractors for the major director $\mathbf{m}_1$ in the vicinity of the two tilted axes in the **CH** motion can be easily identified. An estimate of the maximal Lyapunov exponent was performed with the method used in [16]. Figure 3(b) depicts the stretching factor versus the nondimensional iteration time, after an initial transient. The slope of the function (indicated by the dashed line) at intermediate time gives an estimate of the maximal Lyapunov exponent. This quantity is positive ($\lambda_1 \sim 0.228$) and thus confirms the chaotic motion.

During the chaotic motion, the degrees of orientation oscillate irregularly. The range of oscillation for the largest eigenvalue of the second moment tensor **M** is about 6% while the largest eigenvalue of **N** fluctuates about 8%. The two eigenvalues are plotted versus each other in Fig. 4.

In summary, we have identified various flow-induced states (LR, FA, and OS), periodic motions (MK and FK), chaotic motion, and the representative shear-induced transition sequences in four distinctive parameter regimes, highlighting the drastically different mesoscopic orientational dynamics and structures in plane shear flows compared to the equilibrium phases in quiescent state. It also reveals the loss of commutative symmetry among the second moment tensors in flow-driven states suggesting an enhanced *orientational correlation* among the molecular axes under shear. The stable time-dependent motion and the robust chaotic structure manifest the release of the orientational frustration facilitated by the asymmetric external flow driven effect at the mesoscale.

The research was partially supported by AFOSR Grant No. F49550-08-1-0107 and NSF Grants No. DMS-0605029, No. DMS-0626180, and No. DMS-0724273.

[1] P. G. DeGennes and J. Prost, in *Physics of Liquid Crystals* (Oxford University Press, Oxford, UK, 1993).
[2] M. Doi and S. Edwards, in *Theory of Polymer Dynamics* (Clarendon Press, Oxford, 1986).
[3] A. Rey and M. Denn, Annu. Rev. Fluid Mech. **34**, 233 (2002).
[4] T. C. Lubensky and L. Radzihovsky, Phys. Rev. E **66**, 031704 (2002).
[5] L. A. Madsen, T. J. Dingemans, M. Nakata, and E. T. Samulski, Phys. Rev. Lett. **92**, 145505 (2004).
[6] M. G. Forest, Q. Wang, and R. Zhou, Rheol. Acta **44**, 80 (2004).
[7] M. G. Forest, Q. Wang, and R. Zhou, Rheol. Acta **43**, 17 (2004).
[8] A. M. Sonnet, E. G. Virga, and G. E. Durand, Phys. Rev. E **67**, 061701 (2003).
[9] F. Bisi, E. G. Virga, E. C. Gartland, G. De Matteis, A. M. Sonnet, and G. E. Durand, Phys. Rev. E **73**, 051709 (2006).
[10] E. Berggren, F. L. Tarroni, and C. Zannoni, J. Chem. Phys. **99**, 6180 (1993).
[11] E. Berggren and C. Zannoni, Mol. Phys. **85**, 299 (1995).
[12] J. P. Straley, Phys. Rev. A **10**, 1881 (1974).
[13] Q. Wang, S. Sircar, and H. Zhou, Commun. Math. Sci. **3**, 605 (2005).
[14] M. G. Forest, S. Sircar, Q. Wang, and R. Zhou, Phys. Fluids **18**, 103102 (2006).
[15] L. Longa, P. Grzybowski, S. Romano, and E. Virga, Phys. Rev. E **71**, 051714 (2005).
[16] M. Grosso, R. Keunings, S. Crescitelli, and P. L. Maffettone, Phys. Rev. Lett. **86**, 3184 (2001).